An efficient method for deriving volatility basis sets from thermodenuder and particle levitation data.

Andrey Khlystov *

Desert Research Institute, 2215 Raggio Parkway, Reno, NV 89512

June 11, 2026

This manuscript has been submitted to Aerosol Science and Technology but has not been peer-reviewed yet. Subsequent versions of this manuscript could have slightly different content. If accepted, the final version of the manuscript will be available via the DOI link on this page.

Abstract

Deriving a volatility basis set (VBS) from measurements of particle evaporation in a thermodenuder or single-particle levitation apparatus has traditionally relied on repeated numerical solution of the evaporation equations to find the VBS that best reproduces observed particle sizes. This approach is computationally demanding and offers little insight into the factors that control the retrieval. Building on the characteristic-time framework of Khlystov [2024], it is shown that the mass fraction remaining of each volatility bin can be expressed through a single integral evaluated directly from the measured particle-size evolution. This reduces VBS retrieval to a constrained linear inversion, eliminating iterative integration of differential equations and making the method about four orders of magnitude faster than the conventional approach. The temperature dependence of the saturation concentration and Kelvin effect is included in the inversion, and the enthalpy of vaporization may be prescribed per bin or retrieved as a single volatility-dependence parameter. Applied to thermodenuder thermograms measured at Duke Forest, NC, and Reno, NV, the method reproduces the VBS obtained with the conventional technique while requiring milliseconds rather than minutes. Using synthetic measurements, we quantify the method's accuracy and sensitivity to assumed surface tension and thermogram temperature resolution. The ambient thermograms constrain the enthalpy of vaporization dependence on bin volatility to be much weaker than the commonly assumed parameterization, with a steep dependence incompatible with the gradual evaporation observed. The method enables rapid processing of large volatility datasets and provides guidance for the design of evaporation measurements.

*E-mail: andrey.khlystov@dri.edu; Corresponding author

1 Introduction

The volatility of its constituents controls the gas-particle partitioning of an aerosol and, with it, the atmospheric fate, lifetime, and reactivity of individual compounds [Seinfeld and Pandis, 2006, George et al., 2015, Shrivastava et al., 2017, Carlton et al., 2020]. Atmospheric aerosols, however, contain thousands of compounds for which the thermodynamic properties are largely unknown [Bilde et al., 2014], and a comparable complexity is found in other applications that depend on multicomponent evaporation, such as spray drying, combustion fuel delivery, and aerosolized drug delivery [Martin et al., 2005, Sazhin, 2017, Tikkanen et al., 2019]. To make volatility-related calculations manageable, such mixtures are commonly represented by a volatility basis set (VBS), in which the components are lumped into a set of surrogate compounds whose saturation concentrations differ by an order of magnitude and which are assumed to form a quasi-ideal mixture obeying absorptive partitioning theory [Donahue et al., 2006, Pankow, 1994]. This representation is now used in many atmospheric chemical transport models [Lane et al., 2008, Murphy and Pandis, 2009, Ahmadov et al., 2012, Jo et al., 2013, Koo et al., 2014].

A VBS is most often obtained experimentally from the evolution of particle size or mass during evaporation, measured either in a thermodenuder (TD) [Cappa, 2010, Fuentes and McFiggans, 2012, Riipinen et al., 2010, Saha et al., 2017] or in a single-particle levitation apparatus [Krieger et al., 2012, Cai et al., 2015]. Retrieving the VBS from such data has traditionally required repeatedly solving the set of ordinary differential equations (ODEs) that govern the evaporation of the individual components until the predicted sizes match the measurements [Seinfeld and Pandis, 2006]. Besides being computationally demanding for large datasets, this fitting is sensitive to the assumed thermodynamic and kinetic parameters – in particular the enthalpy of vaporization and the accommodation (evaporation) coefficient, which are seldom known *a priori* [Cappa and Jimenez, 2010] – and to measurement noise, both of which can introduce large uncertainties into the derived VBS [Karnezi et al., 2014].

The opaque nature of these numerical solutions also makes it difficult to discern how the various factors govern the retrieval, or to anticipate, when designing an experiment, the evaporation time or temperature range required to cover a given volatility range and the time or temperature resolution needed to resolve it.

The evaporation of individual compounds from such a mixture, and the effect of the mixture composition on their evaporation times, were analyzed in a previous study [Khlystov, 2024]. It was shown there that the time evolution of the mass fraction remaining of any compound is controlled mostly by its characteristic evaporation time and can be derived from that of any other component in the mixture. In this paper, that framework is used to develop a new approach to deriving a VBS from the measured particle size changes at different times or temperatures. The new approach does not require a numerical solution of ordinary differential equations and is thus much faster, allowing quick processing of a large number of observations. How experimental condi-

tions and assumed parameters affect the measurable saturation concentration range is also discussed.

2 Theory

2.1 Evaporation kinetics of individual compounds

Let us consider evaporation of a single particle composed of an arbitrary number of components that form an ideal, well-mixed liquid solution, i.e., with all activity coefficients equal to unity and no inter-particle transfer limitations of the kind found in solid or highly viscous particles [Li and Shiraiwa, 2019]; such an assumption holds well for most conditions encountered in the lower troposphere [Reid et al., 2018]. More generally, the particle may contain a non-volatile, inert core that does not exchange material with the volatile shell. As in previous experimental studies of aerosol volatility [Cappa, 2010, Fuentes and McFiggans, 2012, Riipinen et al., 2010, Saha et al., 2017] and in the characteristic-time analysis on which the present method builds [Khlystov, 2024], all components of the volatile mixture are assumed to share the same molecular weight (M), density (ρ), surface tension, and evaporation coefficient (α). As discussed below, the equal-molecular-weight assumption is what allows the evaporation integral to be evaluated directly from the measured particle sizes; the more general treatment, in which the molecular weight varies between components, is given by Khlystov [2024]. Evaporation is further assumed to occur in a vapor-free environment, where the gas-phase concentration of every component is kept at zero – as realized when the vapor is continuously stripped (a diffusion denuder, or a particle levitated in a clean gas stream) or when the aerosol is strongly diluted or heated so that the initial loading is negligible relative to the equilibrium vapor concentration, as in a TD [Khlystov, 2024].

The evaporation rate of component i in vapor-free conditions (i.e., the vapor concentration in the gas phase is zero) is proportional to its saturation vapor concentration (C_i), diffusion coefficient (D_i), and its molar fraction in the mixture, which is equal, under the assumption of identical molecular weights, to the ratio of its mass, m_i, and the volatile material mass, m_v [Seinfeld and Pandis, 2006]:

$$\frac{\mathrm{d}m_i}{\mathrm{d}t} = -2\pi D_i d F(d) K(d) C_i \frac{m_i}{m_v}, \tag{1}$$

where d is the particle size. $F(d)$ is the Fuchs-Sutugin correction factor [Fuchs and Sutugin, 1971]:

$$F(d) = \frac{0.75\alpha(1+Kn)}{Kn^2 + Kn + 0.283\alpha Kn + 0.75\alpha}, \tag{2}$$

in which Kn is the Knudsen number ($Kn = 2\lambda/d$, with λ being the mean free path of the evaporating species). $K(d)$ is the Kelvin effect correction:

$$K(d) = \exp\left(\frac{4\sigma M}{\rho R T d}\right), \tag{3}$$

where σ is the surface tension, R is the universal gas constant, and T is temperature.

As shown in Section S1.1, Eq.1 can be rewritten in terms of the mass fraction remaining of component i ($x_i = m_i/m_{i,0}$, where $m_{i,0}$ is its initial mass):

$$\frac{\mathrm{d}\log(x_i)}{\mathrm{d}t} = -\tau_i^{-1} \left(1 + z_n\left(\frac{\rho_n}{\rho_v} - 1\right)\right) \frac{z^{1/3}}{z - z_n} F(z, d_0)K(z, d_0), \tag{4}$$

where z is the volume fraction remaining, z_n is the initial volume fraction of the non-volatile material, d_0 is the initial particle diameter, ρ_n is density of the non-volatile core, ρ_v is the density of the volatile material, and τ_i is the characteristic time:

$$\tau_i = \frac{\rho_0 d_0^2}{12 D_i C_i}, \tag{5}$$

in which ρ_0 is the particle density before evaporation; it is given by Eq.S2.

If there is no non-volatile core, Eq.4 reduces to:

$$\frac{\mathrm{d}\log(x_i)}{\mathrm{d}t} = -\tau_i^{-1} \frac{F(z, d_0)K(z, d_0)}{z^{2/3}}. \tag{6}$$

By separating variables and integrating, we obtain an expression describing the time evolution of x_i:

$$\log(x_i) = -\frac{I(t)}{\tau_i}, \tag{7}$$

where $I(t)$ in the case of non-volatile core is:

$$I(t) = \left(1 + z_n\left(\frac{\rho_n}{\rho_v} - 1\right)\right) \int_0^t \frac{z^{1/3}}{z - z_n} F(z, d_0)K(z, d_0)\mathrm{d}t. \tag{8}$$

In the case of no non-volatile core, it is:

$$I(t) = \int_0^t \frac{F(z, d_0)K(z, d_0)}{z^{2/3}}\mathrm{d}t \tag{9}$$

The key implication of Equation 7 is that the mass fraction remaining of any compound in a mixture can be calculated for any moment in time if the compound characteristic time, τ_i, and the time evolution of the particle size (or the volume fraction remaining), and thus $I(t)$, are known. It should be noted that $I(t)$ does not depend on the compound; it is a single function common to all components of the mixture, so that the mass fractions remaining of any two compounds are interrelated through the ratio of their characteristic times [Khlystov, 2024]. The time evolution of particle size is routinely measured in single particle levitation techniques [Davis, 1997, Reid, 2009, Krieger et al., 2012], which provides direct means to evaluate $I(t)$, if other parameters needed for calculation of the integral (the accommodation coefficient, surface tension, etc.) are known or assumed. After $I(t)$ is evaluated, x_i can be easily calculated using Eq.7, which in turn can be used to derive the VBS, as will be discussed below. It will be also shown that TD techniques that usually vary temperature while keeping evaporation time constant can also be used to derive the VBS using Eq.7.

2.2 VBS derivation using time evolution of particle size

To derive the VBS from a time sequence of measured particle sizes, the following steps should be taken. If a set of N particle diameters $(d_0, d_1, ..., d_{N-1})$ was measured at the corresponding times $(t_0, t_1, ..., t_{N-1})$, a set of values of $I(t)$ can be calculated using Equation 8 or 9 and one of the Newton-Cotes formulas [Tanton, 2005]. For example, for a particle without a non-volatile core, the trapezoid rule produces the following formula:

$$\begin{aligned} I_n &= d_0^2 \int_0^{t_n} \frac{F(d)K(d)}{d^2} \mathrm{d}t \\ &\approx d_0^2 \sum_{j=1}^{n} \frac{t_j - t_{j-1}}{2} \left(\frac{F(d_j)K(d_j)}{d_j^2} + \frac{F(d_{j-1})K(d_{j-1})}{d_{j-1}^2} \right), \end{aligned} \tag{10}$$

where $1 \leq n \leq N$. At t_0, the integral is obviously zero, i.e., $I_0 = 0$.

The accuracy of the integral approximation will depend on the time resolution of the measurements and the choice of a Newton-Cotes formula: a better accuracy can be achieved with a higher time resolution of the measurements and/or a higher order Newton-Cotes formula.

For a mixture composed of K compounds with saturation vapor concentrations $(C_0, C_1, ..., C_{K-1})$ and diffusion coefficients $(D_0, D_1, ..., D_{K-1})$, a set of characteristic times τ_i can be computed using Equation 5. Then, a $(K \times N)$ matrix of MFR values of individual compounds at each point of time can be calculated using Equation 7:

$$x_{i,n} = \exp\left(-\frac{I_n}{\tau_i}\right), \tag{11}$$

where i is the compound number and n is the observation number.

Since particle diameters at different times t_n are available, volatile particle mass corresponding to each measurement can be calculated using Eq.S3. The initial VBS, i.e., a set of initial mass fractions of individual components in the volatile mixture $(f_0, f_1, ..., f_{K-1})$, can then be found by solving the following matrix equation:

$$\mathrm{M} = m_{v,0}\mathrm{XF}, \tag{12}$$

where M is an N-element array of volatile mass corresponding to each observation, $m_{v,0}$ is the initial mass of volatile material in the particle, X is an $(N \times K)$ matrix of MFR values for VBS bins corresponding to each observation (Eq.11), and F is a K-element array of the VBS values (mass fraction of individual VBS bins) at the start of evaporation.

It should be noted that both X and M are subject to experimental uncertainties, which could result in physically impossible solutions or large fluctuations in F. This can be mitigated by solving Equation 12 using non-negativity and $\sum_i \mathrm{F}_i = 1$ constraints.

2.3 VBS derivation using particle size evolution at different temperatures

Unlike single particle levitation techniques, most TD measurements use observations of particle size at different temperatures while keeping evaporation time constant. In this case, the characteristic time of component i should be corrected for the increase in its diffusion coefficient and its saturation vapor concentration due to a higher temperature T_n during measurement n relative to the temperature of the reference (not heated) measurements, T_0:

$$\tau_{i,n} = \frac{\rho_0 d_0^2}{12 D_{i,n} C_i} \exp\left(-\frac{\Delta H_i}{R}\left(\frac{1}{T_0} - \frac{1}{T_n}\right)\right), \tag{13}$$

in which ΔH_i is the enthalpy of vaporization of component i and $D_{i,n}$ is its diffusion coefficient at temperature T_n.

Estimation of the integral I (Eq.9), however, is less accurate than in the case of isothermal measurements due to the temperature dependence of the $F(d)$ and, especially, $K(d)$ functions. Estimation of the integral I at a given temperature requires knowledge of diameter changes between the start of evaporation and its end at the residence time in the TD. Such data is not available, as only the initial and final sizes are measured for each temperature. However, a fairly accurate estimate could still be achieved using measurements at other temperatures and the same residence time. Measurements at progressively higher temperatures could be considered as measurements at progressively longer "effective" times. If the enthalpy of vaporization is assumed to be the same for all compounds in the mixture, $L_i(T_n) = L(T_n)$ is constant at each measurement point. In this case, Equation 7 can be rewritten as:

$$\log(x_{i,n}) = -\frac{L(T_n) I(t_r)}{\tau_i}, \tag{14}$$

where t_r is the residence time corrected for its decrease with temperature: as the carrier gas is heated it expands, so that at a fixed mass flow the residence time scales as $t_r = t_{res}\, T_0/T_n$, where t_{res} is the residence time at the reference temperature. Since $L(T_n)$ is constant, it can be brought under the integral (see Equation 9), after which a variable substitution can be made, such that the upper integration limit changes to $t_{eff} = L(T_n) t_r$. Equation 7 then becomes $\log(x_i) = -I(t_{eff})/\tau_i$. In other words, measurements at different temperatures can be considered as measurements at different effective residence times. This insight is useful for estimating the range of saturation concentrations that can be investigated within a given temperature range used for TD measurements [Khlystov, 2024].

The assumption that the enthalpy of vaporization is common to all compounds is convenient but not required. If each bin is assigned its own enthalpy ΔH_i, the temperature enhancement of the saturation concentration, $L_i(T_n) = \exp\left[\Delta H_i/R\,(1/T_0 - 1/T_n)\right]$, becomes specific to the bin, and the single effective-time substitution leading to Equation 14 no longer applies. The

geometric part of the integral, however, remains common to all bins, since the functions F and K depend only on the particle size and temperature. It is therefore convenient to evaluate the integral once using a reference enthalpy ΔH_{ref} (for example, the mean of the ΔH_i or the value given by the commonly assumed linear relationship between ΔH_i and $\log_{10} C_i^*$), and to restore the enthalpy of each individual bin through a multiplicative correction $L_i(T_n)/L_{\mathrm{ref}}(T_n)$ applied to the corresponding column of the matrix X. Because ΔH_i enters only the bin-specific characteristic time (Equation 13) and not the shared integral, the matrix Equation 12 remains linear in the VBS, and the same constrained (non-negative, sums-to-one) inversion can be used. This makes it possible to prescribe an arbitrary enthalpy distribution rather than assuming a single value for the entire mixture.

It should be noted that bringing $L(T_n)$ under the integral and treating the heated measurements as samples of a single universal evaporation curve is exact only when the integrand $F(d)K(d)/d^2$ depends on the particle size alone. The Kelvin term, however, has an explicit temperature dependence through Equation 3, so that the factorization leading to Equation 14 is, strictly speaking, approximate. In practice, this dependence can be accounted for by evaluating $K(d)$ at each node of the reconstructed size trajectory using the temperature at which the corresponding size was measured; the temperature dependence of $F(d)$, which enters more weakly through the mean free path and the diffusion coefficient, can be treated in the same manner. Since the Kelvin term grows as the particle shrinks, its contribution is largest for small particles and high surface tensions, and so is the error incurred by the approximation. The accuracy of the retrieved VBS under these conditions is examined in Section 4.3.

After this correction, steps described in Section 2.2 can be used to calculate the VBS with the only difference being that τ_i in Equation 11 should be substituted with $\tau_{i,n}$.

3 Methods

3.1 Calculations

All calculations presented in this paper were done using Python version 3.8, which was part of an Anaconda installation [Anaconda, Inc., 2021] on a MacBook Pro M1 laptop. The following Python packages were used: NumPy v.1.20, SciPy v.1.7, Pandas v.1.3, and Matplotlib v.3.5 [Harris et al., 2020, Virtanen et al., 2020, Wes McKinney, 2010, Hunter, 2007]. Python scripts used for the calculations and for creating the plots in this paper are archived on Zenodo [Khlystov, 2026].

All calculations assumed that the components of the mixture share a common molecular weight, as is commonly done when the molecular weights of the individual constituents are unknown [Cappa, 2010, Riipinen et al., 2010, Khlystov, 2024]. The temperature dependence of the gas-phase diffusion coefficient is weak compared with the Clausius–Clapeyron enhancement of the sat-

uration concentration and was neglected, i.e., the diffusion coefficient was held constant; the change of the residence time with temperature ($t_r = t_{res} T_0/T_n$, Section 2.3) and the temperature dependence of the saturation concentration and the Kelvin term were retained.

3.2 Measurements

To demonstrate the derivation of a VBS from TD measurements using the approach presented in this paper, data collected during two field campaign was used as an example. One thermogram example was measured at the Forest-Atmosphere Carbon Transfer and Storage (FACTS-1) site in the Blackwood Division of Duke Forest near Chapel Hill, NC (35.98N, 79.09W). The site is situated in a field surrounded by a Loblolly Pine plantation, with Interstate 40 running 2.5 km to the southwest as well as several secondary roads running closer to the site. The instruments were housed in an air-conditioned shelter. A volatility tandem differential mobility analyzer (VTDMA) system consisted of a differential mobility analyzer (DMA, Model 3071, TSI, Shoreview, MN, USA) that selected quasi-monodisperse particles of 100 nm in diameter. The selected particles were led into a TD that is described in detail in Saleh et al. [2008]. Briefly, the TD consists of a 1 meter long, 2.5 cm inner diameter (ID) heated stainless-steel tube. The average residence time in the TD at the air flow used in this study was 21.7 s at room temperature. The size distribution of the aerosol after the TD was measured with a scanning mobility particle sizer (SMPS) that consisted of a DMA (Model 3071, TSI, Shoreview, MN, USA) and a condensation particle counter (CPC 3010, TSI, Shoreview, MN, USA). Both DMAs were equipped with Po-210 neutralizers (Aerosol Dynamics, Berkeley, CA, USA) and operated at 10 L min^{-1} sheath flow and 1 L min^{-1} aerosol flow. The SMPS was operated with a 120 s up scan, and a 30 s down scan, providing measurements in the diameter range between 10 and 250 nm. The thermogram used in this paper was measured in the afternoon of June 18, 2015. The TD was heated to 400°C and held at that temperature for 30 minutes, then let passively cool down to about 50°C thus providing a temperature scan.

A second thermogram example was measured in Reno, NV, using the same instrumental setup. The measurements were carried out on the roof of the Desert Research Institute (DRI) building located at 39°34′20.67″N, 119°48′06.83″W, in northern Reno, NV. Reno is a city on the east side of the Sierra Nevada and the west of the Great Basin, with an area of approximately 289 km^2 and a population of about 275,000 in 2023. The elevation of the city is approximately 1300 m above sea level. The thermogram used here was measured on the morning of July 22, 2017, with 100 nm particles selected and their size after the TD measured over a temperature range from 25 to 202°C at a room-temperature residence time of 21.7 s.

4 Results and discussion

4.1 Application to thermodenuder measurements of ambient aerosols

To demonstrate the performance of the procedure described in section 2.3, it was applied to VTDMA measurements of ambient aerosols at Duke Forest near Chapel Hill, NC, USA. The measurement site is influenced by a mixture of biogenic and urban sources with the ambient aerosol containing a large fraction of organic compounds [Bhat and Fraser, 2007].

Panel (a) of Figure 1 shows an example of the measured sizes of a 100 nm aerosol after passing the TD as a function of TD temperature. Panel (b) of the figure shows the VBS derived from these measurements using the method described in Section 2.3 and the conventional way in which particle sizes are numerically calculated for various VBSs to find the one that fits best the observed particle sizes. The VBS bins ranged from -8 to 2 in log-volatility space, which is the range resolvable for these measurement conditions (Section 4.3). The new method produces results that are essentially identical to the conventional method. However, the new method is significantly faster. The VBS shown in panel (b) was derived from the full thermogram; to provide a controlled timing comparison, the thermogram was reduced to 16 points equally spaced in the temperature space, for which the conventional method took 2 min 48 s $\pm$ 12 s while the new method took only 18 ms $\pm$ 1 ms – about 10000 times faster than the conventional method. The reason is that the conventional method requires numerical integration of Eq. 1 for each observed point and a VBS being tested, while the new method does not require any numerical integration; the speed advantage therefore grows with the number of points, exceeding ten thousand on the full thermogram.

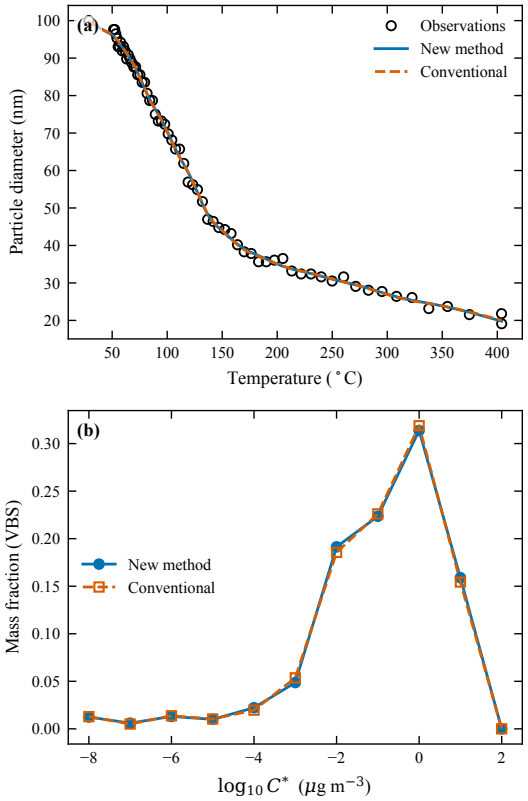

Figure 1: Application to the Duke Forest thermodenuder thermogram. (a) Particle size as a function of TD temperature: measurements (circles) and sizes predicted from the VBS retrieved with the new and the conventional methods. (b) VBS retrieved with the two methods. The enthalpy of vaporization is assumed to be 100 kJ/mol, the evaporation coefficient 0.1, and the surface tension 0.05 J m^{-2}.

To verify that this agreement is not specific to a single dataset, the method was applied to a second thermogram, measured in Reno, NV, on July 22, 2017, in an aerosol influenced by high-desert urban sources. In this case, 100 nm particles were sampled and their size after the TD was measured over a temperature range from 25 to 202°C, with a residence time of 21.7 s at room temperature. Figure 2 shows the measured sizes together with the VBS retrieved using the new and the conventional methods. As for the Duke Forest data, the two methods yield essentially identical volatility distributions and both reproduce the observed sizes to within about 0.5 nm. The retrieval with the new method required 3 ms, compared with 26 s for the conventional method, again a speedup of about four orders of magnitude. The retrieved VBS is dominated by low-volatility material, with the mass peaking near $\log_{10} C^* = 0$ μg m^{-3} and extending down

to $\log_{10} C^* = -6$; no resolved material was found in the most volatile bin, consistent with the most volatile compounds having largely evaporated by the reference measurement.

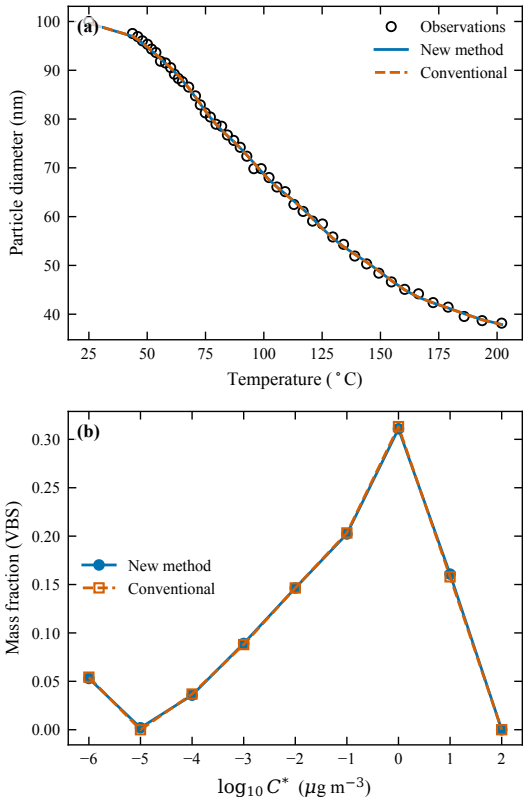

Figure 2: Application to a thermodenuder thermogram measured in Reno, NV. (a) Particle size as a function of TD temperature: measurements (circles) and sizes predicted from the VBS retrieved with the new and the conventional methods. (b) VBS retrieved with the two methods. The enthalpy of vaporization is assumed to be 100 kJ/mol, the evaporation coefficient 0.1, and the surface tension 0.05 J m^{-2}.

The examples above assumed fixed values of the evaporation coefficient and the enthalpy of vaporization. These two parameters cannot be determined from a single temperature- or time-resolved evaporation measurement, and any assumption about their values propagates into the retrieved VBS [Khlystov, 2024]. Figure 3 illustrates this ambiguity by inverting the Reno thermogram under a range of assumed values. A lower evaporation coefficient slows the evaporation, so that a more volatile distribution is required to reproduce the same observed sizes; the retrieved VBS therefore shifts toward higher volatilities while approxi-

mately preserving its shape (panel a). A lower enthalpy of vaporization likewise shifts the retrieved VBS toward higher volatilities, but in this case its shape also changes, becoming narrower (panel b). These dependencies are consistent with the theory reported by Khlystov [2024], who showed that the retrieved VBS depends on the assumed evaporation coefficient and enthalpy of vaporization. Therefore, the retrieved VBS should always be reported together with the assumed evaporation coefficient and enthalpy of vaporization to assure accurate evaporation predictions using the retrieved VBS [Khlystov, 2024].

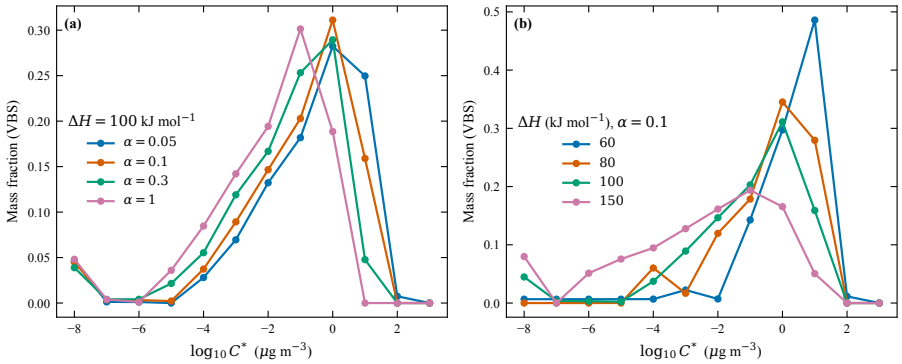

Figure 3: Sensitivity of the VBS retrieved from the Reno thermogram to the assumed evaporation parameters. (a) VBS retrieved for several values of the evaporation coefficient α at a fixed enthalpy of vaporization. (b) VBS retrieved for several values of the enthalpy of vaporization at a fixed evaporation coefficient. Lower α and lower ΔH both shift the retrieved distribution toward higher volatilities.

4.2 Per-bin enthalpy of vaporization

The examples above assumed a single enthalpy of vaporization for all bins. In reality the enthalpy of vaporization tends to decrease with volatility. The method accommodates an arbitrary per-bin value ΔH_i at no additional cost: because ΔH_i enters only through the bin-specific characteristic time while the geometric and Kelvin integral remains common to all bins (Section 2.3), the inversion remains a single linear solution. Figure 4a demonstrates this on synthetic data. A known VBS was used to calculate a thermogram using a per-bin enthalpy following the semi-empirical correlation of Epstein et al. [2010], $\Delta H_i = 131 - 11 \log_{10} C_i^*$ kJ mol^{-1}, in which the least volatile bins have the highest enthalpy. Inverting with the same per-bin enthalpy recovers the true VBS almost exactly (root-mean-square error of the retrieved mass fractions, RMSE 2.1×10^{-3}), whereas inverting the same measurements with a single enthalpy equal to the mean of the ΔH_i biases the retrieval by more than an order of magnitude (RMSE 6.5×10^{-2}), shifting mass toward the center of the distribution.

Application of the per-bin enthalpy to the ambient data reveals an interesting phenomenon. The Reno thermogram is reproduced to a size RMSE of 0.46 nm by a constant $\Delta H = 100$ kJ mol^{-1}, but the steep Epstein et al. [2010] law cannot reproduce it at all, leaving a size RMSE of about 26 nm; the exact conventional inversion fails in the same way (a residual of about 27 nm), confirming that this is a property of the data and not of the fast method. This holds for the Epstein correlation in its original published form, with both the intercept (131 kJ mol^{-1}) and the slope (11 kJ mol^{-1} per decade) as given, and is therefore not an artifact of how the mean enthalpy is fixed; holding the mean enthalpy at 100 kJ mol^{-1} and varying only the slope produces an almost identical misfit (Figure 4c), confirming that it is the steep volatility dependence of the enthalpy, rather than its absolute magnitude, that is incompatible with the data. The reason is apparent in Figure 4b: a steep enthalpy makes each bin evaporate over a narrow temperature interval, so the predicted particle size collapses near 120°C and cannot reproduce the gradual, high-temperature tail of the measured thermogram. Figure 4c quantifies the constraint by varying the slope of the ΔH–$\log_{10} C^*$ relation while holding the mean enthalpy fixed. Both thermograms are reproduced only for slopes well below the Epstein et al. [2010] value of about 11 kJ mol^{-1} per decade; the Reno data tolerate slopes up to roughly 5 kJ mol^{-1} per decade, while the Duke data, measured up to 400°C with near-complete evaporation, constrain the slope to be still smaller. The data themselves therefore bound the volatility dependence of the enthalpy of vaporization, and the speed of the method makes such an exploration computationally affordable. While the per-bin enthalpies can be prescribed explicitly, a convenient alternative is to constrain them to the linear law above and treat its slope as a single free parameter, retrieved by minimizing the size residual. The full joint retrieval of an unknown enthalpy for every bin together with the VBS is ill-posed, because the enthalpy and the saturation concentration are partly degenerate; restricting the enthalpy to a one-parameter law regularizes the problem and turns the data into an estimate of the slope. Fitted in this way, the slope is about 1.5 kJ mol^{-1} per decade for the Reno thermogram and essentially zero for the Duke thermogram, corresponding to an enthalpy of vaporization that is nearly independent of volatility over the measured range and much weaker than the Epstein et al. [2010] correlation.

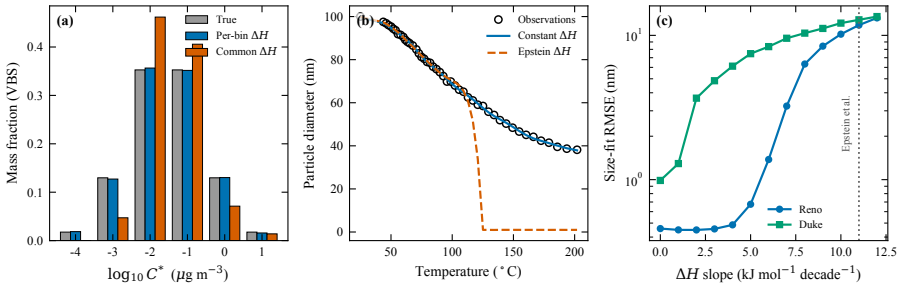

Figure 4: Per-bin enthalpy of vaporization. (a) Synthetic test: a known VBS generated with a per-bin enthalpy following Epstein et al. [2010] is recovered when inverted with the same per-bin enthalpy, but is biased when inverted with a single common enthalpy equal to the mean. (b) Reno thermogram reproduced with a constant enthalpy of vaporization and with the steep per-bin Epstein law, which collapses the particle near 120°C. (c) Size-fit RMSE as a function of the slope of the ΔH–$\log_{10} C^*$ relation (mean enthalpy fixed at 100 kJ mol^{-1}) for the Reno and Duke thermograms; the dotted line marks the Epstein slope.

4.3 Accuracy and sensitivity of the method

The application to ambient data demonstrates that the new method reproduces the VBS obtained with the conventional approach. To characterize its accuracy more systematically and to examine its sensitivity to the measurement resolution and to the assumed surface tension, a series of synthetic experiments was performed. In each experiment, a known VBS was prescribed and the corresponding evolution of the particle size was computed with the conventional numerical model (Section S1.2), which integrates Equation 1 directly and therefore includes the full size and temperature dependence of the Fuchs-Sutugin and Kelvin corrections. The resulting sizes were then sampled at a finite number of points and inverted with the new method. Since the true VBS is known, the retrieval error can be quantified directly; it is reported here as the root-mean-square error (RMSE) of the retrieved mass fractions relative to the prescribed values.

Let us first consider isothermal measurements, in which the particle size is followed in time at a constant temperature, as in single-particle levitation techniques [Davis, 1997, Reid, 2009, Krieger et al., 2012]. A seven-bin VBS spanning saturation concentrations from 0.1 to 100 μg m^{-3} was assigned to a 100 nm particle evaporating at 25°C with a surface tension of 0.05 J m^{-2}, and its size was followed over a time window from 0.2 to 10^4 s. Figure 5 shows the retrieval error as a function of the number of sampling points for two sampling strategies: points spaced uniformly in time and points spaced uniformly in the logarithm of time. Logarithmic spacing is markedly more efficient. It reaches an RMSE of about 10^{-3} with as few as ten points, whereas uniform spacing requires several times as many points to achieve a comparable accuracy and remains roughly an

order of magnitude less accurate at any given number of points. This behavior reflects the logarithmic nature of the volatility distribution: evenly spaced volatility bins evaporate over time intervals that are themselves approximately logarithmically distributed, so that logarithmic sampling captures the evaporation of all bins with comparable fidelity. For a given number of measurements, the volatility range that can be resolved is therefore maximized by sampling the evaporation at logarithmically spaced times.

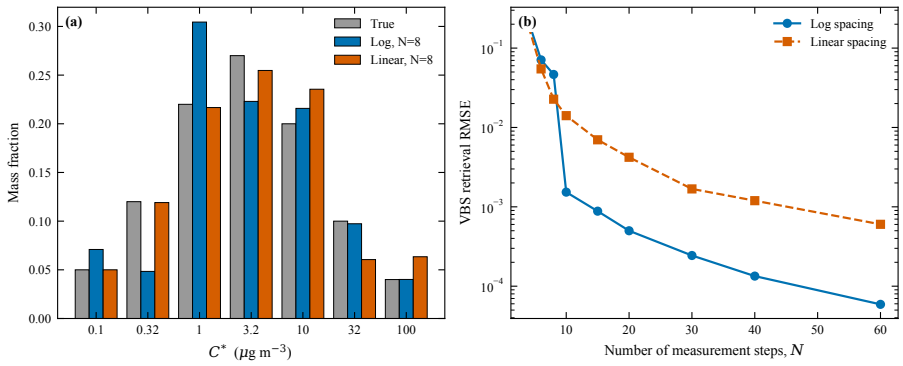

Figure 5: Isothermal sensitivity to the measurement step size. (a) VBS retrieved from synthetic measurements sampled at eight points spaced uniformly in time (linear) and in the logarithm of time (log), compared to the true VBS. (b) RMSE of the retrieved VBS as a function of the number of sampling points for the two sampling strategies.

Now let us consider TD measurements, in which the particle size is measured at a fixed residence time over a range of temperatures. Here the accuracy of the method is governed by two factors: the number of temperature steps and the magnitude of the Kelvin term, which is in turn controlled by the assumed surface tension. The surface tension of organic aerosols is not well constrained; reported values for typical organic mixtures lie in the range of about 0.03 to 0.05 J m^{-2}, while considerably higher values are sometimes used. To examine the combined effect of these two factors, a six-bin VBS spanning whole decades of $\log_{10} C^*$ from -4 to 1 – placed within the resolvable volatility range of -5 to 2 predicted for these conditions by the analysis of Khlystov [2024] – was retrieved over a grid of surface tensions (from 0.02 to 0.20 J m^{-2}) and numbers of temperature steps (from 8 to 64), for a 100 nm particle measured between 25 and 200°C with a residence time of 21.7 s and an enthalpy of vaporization of 100 kJ mol^{-1}, matching the conditions of the ambient measurements above. The surface tension used in the inversion was set equal to that used to generate the synthetic measurements, so that the reported error reflects the intrinsic approximation error of the method rather than a bias introduced by an incorrectly assumed surface tension. Figure 6 shows the resulting RMSE. The error increases monotonically with surface tension, roughly doubling over the range

examined, because a larger Kelvin term makes the integrand more strongly dependent on temperature and the effective-time approximation (Section 2.3) correspondingly less exact. The error decreases with the number of temperature steps and essentially saturates beyond about twelve steps, at which point the temperature resolution is no longer limiting. The two factors interact, in that the penalty associated with coarse resolution grows with the surface tension. The retrieval error is, however, remarkably small throughout: the RMSE of the retrieved mass fractions never exceeds about 2×10^{-3} (roughly 0.2%) anywhere on the grid, and stays below 1.6×10^{-3} once at least twelve temperature steps are used; the least favorable case examined here, the highest surface tension combined with only eight temperature steps, still gives an RMSE of only 2.3×10^{-3}. With the surface tension correctly specified, then, the intrinsic approximation error of the method is negligible across the whole range of surface tensions considered. Whether the surface tension needs to be known at all is examined next.

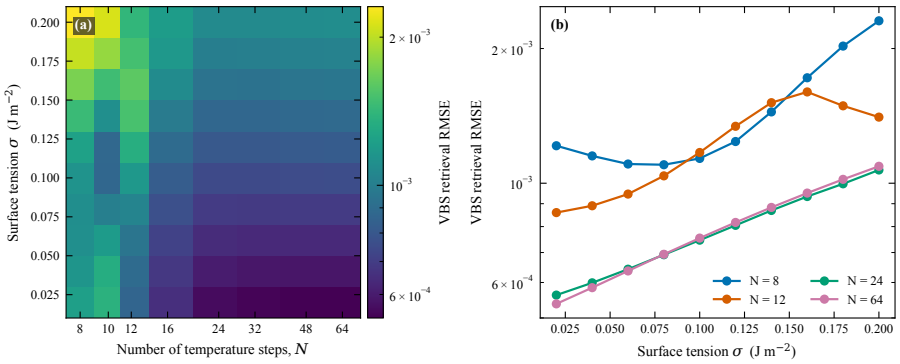

Figure 6: Thermodenuder sensitivity to surface tension and measurement resolution. (a) RMSE of the retrieved VBS as a function of the number of temperature steps and the surface tension. (b) RMSE as a function of surface tension for selected numbers of temperature steps. The surface tension used in the inversion equals that used to generate the synthetic measurements, so the error reflects the intrinsic approximation error of the method.

The analysis above isolates the intrinsic approximation error by assuming the surface tension is known. Because the surface tension is in fact poorly constrained, the next question is how much the retrieval is degraded when the value assumed in the inversion differs from the true one. The synthetic experiment was repeated at a fixed resolution of twenty-four temperature steps – well beyond the point at which resolution ceases to limit the accuracy – with the measurements generated at one surface tension and inverted with another, each spanning the same 0.02 to 0.20 J m^{-2} range. Figure 7 shows the result. Within the realistic range for organic aerosol (0.03 to 0.05 J m^{-2}), the assumed surface tension is immaterial: the RMSE stays at or below 2×10^{-3} regardless of the mismatch,

indistinguishable from the intrinsic error of the matched case. The retrieval degrades appreciably only when the assumed surface tension is grossly overestimated toward the higher values sometimes used in the literature; inverting at 0.20 J m^{-2} measurements generated at 0.05 J m^{-2} – a fourfold overestimate – raises the RMSE to about 1.6×10^{-2} and shifts the retrieved mass toward lower volatility, as expected from the larger assumed Kelvin term. It can therefore be concluded that the method does not require the surface tension to be known: any value within the realistic range recovers the VBS essentially as accurately as the true one, and only an implausibly high assumed surface tension introduces a noticeable bias.

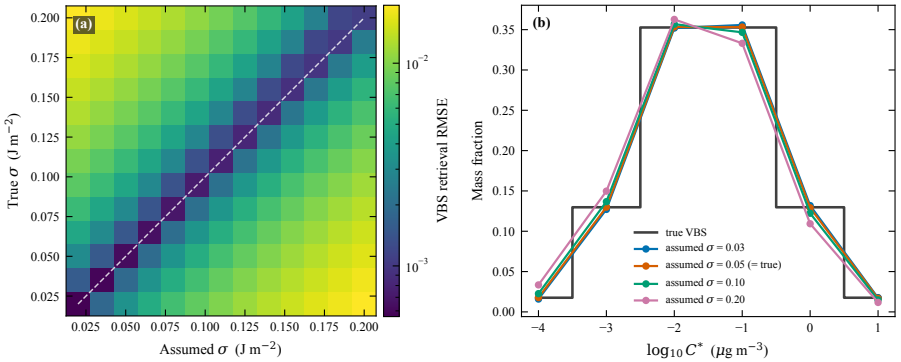

Figure 7: Sensitivity of the retrieval to a misspecified surface tension, at a fixed resolution of twenty-four temperature steps. (a) RMSE of the retrieved VBS as a function of the true surface tension (used to generate the synthetic measurements) and the surface tension assumed in the inversion; the dashed diagonal marks the matched case of Figure 6. (b) VBS retrieved for measurements generated at $\sigma = 0.05$ J m^{-2} and inverted with several assumed surface tensions, compared with the true VBS. Within the realistic range (0.03 to 0.05 J m^{-2}) the retrieval is insensitive to the assumed value; only a gross overestimate biases it toward lower volatility.

The accuracy of the method at high surface tension relies on evaluating the Kelvin term at the local temperature of each measurement, as described in Section 2.3. If the Kelvin term is instead evaluated at a single reference temperature, the retrieval error grows roughly six times faster with surface tension and the retrieved VBS becomes biased at high surface tension. This comparison is presented in the Supplement (Figure S1).

These results, together with the resolution analysis of Khlystov [2024], lead to a simple recommendation for the minimum number of measurement points needed to resolve a VBS at the conventional resolution of one decade in C^*. The number of points is set by the volatility range to be covered and by the resolution required within it. For isothermal measurements, the saturation concentration that can be resolved is fixed by the measurement time, and Figure 5 shows that

about ten points spaced uniformly in the logarithm of time are sufficient to recover a VBS spanning three decades, or roughly three points per decade; points spaced uniformly in time are markedly less efficient and should be avoided. For thermodenuder measurements, the temperature step required to separate two bins differing by a decade in volatility is approximately $\ln(10)\, RT^2/\Delta H$ [Khlystov, 2024], which for $\Delta H = 100$ kJ mol^{-1} ranges from about 17 K near room temperature to about 43 K at 200°C. Resolving the full window therefore requires steps no coarser than this local value, with the points concentrated toward the lower temperatures where the decadal step is smallest; in the example above, about twelve steps across the 25–200°C ramp were sufficient to resolve the six-decade volatility window, again roughly two points per decade. As a practical rule, at least two measurement points are needed per decade of volatility, never fewer than the number of VBS bins, with the points placed so as to sample the volatility space approximately uniformly – logarithmically in time for isothermal measurements, and with a temperature spacing that accounts for the T^2 growth of the decadal step for thermodenuder measurements.

5 Conclusions

This paper presents a new method for deriving a VBS from particle sizes or mass measured at different times (as done in particle levitation techniques) or at different temperatures (as done in TD measurements). The method builds on the result that the mass fraction remaining of any compound in a well mixed, quasi-ideal mixture is controlled mostly by its characteristic evaporation time, which is inversely proportional to the compound saturation concentration [Khlystov, 2024]. This allows the mass fraction remaining of each volatility bin to be expressed through an integral, $I(t)$, that is evaluated directly from the measured evolution of the particle size, thereby reducing the VBS retrieval to a single constrained linear inversion rather than a repeated numerical solution of a set of ODEs.

VBS derived with the new method closely match those obtained with the conventional approach to TD data analysis, in which a set of ODEs is solved for different VBS to select the one that best matches the measurements. The new method is much faster than the conventional method, allowing quick processing of large datasets.

The characteristic-time framework underlying the method can also be used to estimate the measurement times or temperature ranges necessary to cover a certain volatility range, as well as the time or temperature step resolution necessary to resolve volatility bins separated by an order of magnitude [Khlystov, 2024]. Measurements in which either the evaporation time or temperature is varied cannot resolve a VBS without assuming the enthalpy of vaporization or the evaporation coefficient. A reduction in the assumed evaporation coefficient causes the derived VBS to shift to higher volatility bins, while the VBS shape is mostly preserved. Likewise, lowering the assumed enthalpy of vaporization shifts the VBS to higher volatility bins; its shape, however, becomes narrower.

In contrast to the enthalpy of vaporization and the evaporation coefficient, the surface tension need not be known: synthetic tests show that any value within the realistic range for organic aerosol recovers the VBS essentially as accurately as the true one, so this comparatively poorly constrained parameter is not a practical limitation. The ambiguity of the VBS shape due to ΔH uncertainty is of little practical importance for aerosol temperature sensitivity as long as the modeling employs the same parameters (ΔH and α) used for the VBS derivation. However, these assumptions have a strong effect on aerosol behavior upon dilution. To better constrain the VBS, measurements at different temperatures need to be supplemented by measurements at either different evaporation times or by measurements of aerosol evaporation under isothermal dilution.

Because the enthalpy of vaporization enters only through the bin-specific characteristic time, the method accommodates an enthalpy that differs from bin to bin, either prescribed explicitly or constrained to a linear dependence on volatility whose slope is retrieved as a single parameter. Applying this to the ambient thermograms reveals that the data themselves limit how strongly the enthalpy may vary with volatility: the steep, commonly used correlation of Epstein et al. [2010] cannot reproduce the observed gradual evaporation – a failure shared by the conventional inversion and therefore inherent to the data – and the retrieved slope is close to zero, indicating an enthalpy that is nearly independent of volatility over the measured range. This suggests that enthalpy–volatility correlations derived for pure compounds should be applied to ambient volatility measurements with caution, and that the speed of the present method makes it practical to test such assumptions against each dataset rather than imposing them.

Acknowledgements

The author thanks Drs. R. Subramanian and C. Bhattarai for their assistance during the ambient measurements.

Funding

This work was supported by the U.S. National Science Foundation under Award No. OIA-2148788, the National Institute of Environmental Health Sciences of the National Institutes of Health under Award No. R01ES029528; and the U.S. Environmental Protection Agency's Science to Achieve Results (STAR) program under Grant No. 83541101. The content is solely the responsibility of the author and does not necessarily represent the official views of the National Institutes of Health or the U.S. Environmental Protection Agency.

Disclosure statement

The author reports there are no competing interests to declare.

Author contributions

Andrey Khlystov: Conceptualization, Methodology, Software, Formal analysis, Investigation, Writing – original draft, Writing – review & editing, Funding acquisition.

Data availability statement

The Python code implementing the method described in this paper, together with the thermodenuder thermograms from Duke Forest, NC, and Reno, NV, that support the findings of this study, is openly available on Zenodo at `https://doi.org/10.5281/zenodo.20634979` [Khlystov, 2026]. The code is also developed and maintained on GitHub at `https://github.com/akhlystov/vbs-td-inversion`.

ORCID

Andrey Khlystov `http://orcid.org/0000-0001-9606-3919`

References

R Ahmadov, SA McKeen, AL Robinson, R Bahreini, AM Middlebrook, JA De Gouw, J Meagher, E-Y Hsie, E Edgerton, S Shaw, et al. A volatility basis set model for summertime secondary organic aerosols over the eastern united states in 2006. *Journal of Geophysical Research: Atmospheres*, 117 (D6), 2012.

Anaconda, Inc. Anaconda software distribution, 2021. URL `https://docs.anaconda.com/`.

Shagun Bhat and Matthew P Fraser. Primary source attribution and analysis of α-pinene photooxidation products in duke forest, north carolina. *Atmospheric Environment*, 41(14):2958–2966, 2007.

M. Bilde, K. Barsanti, M. Booth, C. Cappa, N. Donahue, G. McFiggans, U.K. Krieger, C. Marcolli, D. Topping, P. Ziemann, M. Barley, S. Clegg, B. Dennis-Smither, E.U. Emanuelson, M. Hallquist, A.M. Hallquist, A. Khlystov, M. Kulmala, D. Mogensen, C.J. Percival, F. Pope, J.P. Reid, M.A.V. Ribeiro da Silva, T. Rosenoern, K. Salo, V.P. Soonsin, T. Yli-Juuti, N. Prisle, J. Pagels, J. Rarey, A. Zardini, and I. Riipinen. Saturation vapor pressures and transition enthalpies of low volatility organic molecules of atmospheric relevance: from dicarboxylic acids to complex mixtures. *Chemical Reviews*, Under review, 2014.

Chen Cai, David J Stewart, Jonathan P Reid, Yun-hong Zhang, Peter Ohm, Cari S Dutcher, and Simon L Clegg. Organic component vapor pressures and

hygroscopicities of aqueous aerosol measured by optical tweezers. *The Journal of Physical Chemistry A*, 119(4):704–718, 2015.

C.D. Cappa. A model of aerosol evaporation kinetics in thermodenuders. *Atmospheric Measurement Techniques*, 3:579–592, 2010.

C.D. Cappa and J.L. Jimenez. Quantitative estimates of the volatility of ambient organic aerosol. *Atmospheric Chemistry and Physics*, 10:5409–5424, 2010.

Annmarie G Carlton, Amy E Christiansen, Madison M Flesch, Christopher J Hennigan, and Neha Sareen. Multiphase atmospheric chemistry in liquid water: impacts and controllability of organic aerosol. *Accounts of Chemical Research*, 53(9):1715–1723, 2020.

E James Davis. A history of single aerosol particle levitation. *Aerosol science and technology*, 26(3):212–254, 1997.

N. M. Donahue, A. L. Robinson, C. O. Stanier, and S. N. Pandis. Coupled partitioning, dilution, and chemical aging of semivolatile organics. *Environmental Science & Technology*, 40(8):2635–2643, 2006.

Scott A. Epstein, Ilona Riipinen, and Neil M. Donahue. A semiempirical correlation between enthalpy of vaporization and saturation concentration for organic aerosol. *Environmental Science & Technology*, 44(2):743–748, 2010. doi: 10.1021/es902497z.

N.A. Fuchs and A.G. Sutugin. *High dispersed aerosols. In Topics in Current Aerosol Research*, volume 2. Pergamon Press, Oxford, 1971.

E. Fuentes and G. McFiggans. A modeling approach to evaluate the uncertainty in estimating the evaporation behaviour and volatility of organic aerosols. *Atmospheric Measurement Techniques*, 5:735–757, 2012.

Christian George, Markus Ammann, Barbara D'Anna, DJ Donaldson, and Sergey A Nizkorodov. Heterogeneous photochemistry in the atmosphere. *Chemical reviews*, 115(10):4218–4258, 2015.

Charles R. Harris, K. Jarrod Millman, Stéfan J. van der Walt, Ralf Gommers, Pauli Virtanen, David Cournapeau, Eric Wieser, Julian Taylor, Sebastian Berg, Nathaniel J. Smith, Robert Kern, Matti Picus, Stephan Hoyer, Marten H. van Kerkwijk, Matthew Brett, Allan Haldane, Jaime Fernández del Río, Mark Wiebe, Pearu Peterson, Pierre Gérard-Marchant, Kevin Sheppard, Tyler Reddy, Warren Weckesser, Hameer Abbasi, Christoph Gohlke, and Travis E. Oliphant. Array programming with NumPy. *Nature*, 585 (7825):357–362, September 2020. doi: 10.1038/s41586-020-2649-2. URL `https://doi.org/10.1038/s41586-020-2649-2`.

J. D. Hunter. Matplotlib: A 2d graphics environment. *Computing in Science & Engineering*, 9(3):90–95, 2007. doi: 10.1109/MCSE.2007.55.

DS Jo, RJ Park, MJ Kim, and DV Spracklen. Effects of chemical aging on global secondary organic aerosol using the volatility basis set approach. *Atmospheric Environment*, 81:230–244, 2013.

E Karnezi, Ilona Riipinen, and SN Pandis. Measuring the atmospheric organic aerosol volatility distribution: a theoretical analysis. *Atmospheric Measurement Techniques*, 7(9):2953–2965, 2014.

Andrey Khlystov. On evaporation kinetics of multicomponent aerosols: Characteristic times and implications for volatility measurements. *Aerosol Science and Technology*, 58(10):1194–1205, 2024. doi: 10.1080/02786826.2024.2385640.

Andrey Khlystov. Efficient derivation of volatility basis sets from thermodenuder and particle levitation data: code and data, 2026. URL `https://doi.org/10.5281/zenodo.20634979`. DOI to be assigned upon release.

Bonyoung Koo, Eladio Knipping, and Greg Yarwood. 1.5-dimensional volatility basis set approach for modeling organic aerosol in camx and cmaq. *Atmospheric Environment*, 95:158–164, 2014.

Ulrich K Krieger, Claudia Marcolli, and Jonathan P Reid. Exploring the complexity of aerosol particle properties and processes using single particle techniques. *Chemical Society Reviews*, 41(19):6631–6662, 2012.

Timothy E Lane, Neil M Donahue, and Spyros N Pandis. Simulating secondary organic aerosol formation using the volatility basis-set approach in a chemical transport model. *Atmospheric Environment*, 42(32):7439–7451, 2008.

Ying Li and Manabu Shiraiwa. Timescales of secondary organic aerosols to reach equilibrium at various temperatures and relative humidities. *Atmospheric Chemistry and Physics*, 19(9):5959–5971, 2019.

Andrew R Martin, Daniel Y Kwok, and Warren H Finlay. Investigating the evaporation of metered-dose inhaler formulations in humid air: single droplet experiments. *Journal of aerosol medicine*, 18(2):218–224, 2005.

Benjamin N Murphy and Spyros N Pandis. Simulating the formation of semivolatile primary and secondary organic aerosol in a regional chemical transport model. *Environmental science & technology*, 43(13):4722–4728, 2009.

J. F. Pankow. An absorption-model of gas-particle partitioning of organic-compounds in the atmosphere. *Atmospheric Environment*, 28(2):185–188, 1994.

Jonathan P Reid. Particle levitation and laboratory scattering. *Journal of Quantitative Spectroscopy and Radiative Transfer*, 110(14-16):1293–1306, 2009.

Jonathan P Reid, Allan K Bertram, David O Topping, Alexander Laskin, Scot T Martin, Markus D Petters, Francis D Pope, and Grazia Rovelli. The viscosity of atmospherically relevant organic particles. *Nature communications*, 9(1): 1–14, 2018.

I. Riipinen, J.R. Pierce, N.M. Donahue, and S.N. Pandis. Equilibration time scales of organic aerosol inside thermodenuders: Evaporation kinetics versus thermodynamics. *Atmospheric Environment*, 44:597–607, 2010.

Provat K Saha, Andrey Khlystov, Khairunnisa Yahya, Yang Zhang, Lu Xu, Nga L Ng, and Andrew P Grieshop. Quantifying the volatility of organic aerosol in the southeastern us. *Atmospheric Chemistry and Physics*, 17(1): 501–520, 2017.

R. Saleh, Walker J., and Khlystov A. Determination of saturation pressure and enthalpy of vaporization of semi-volatile aerosols: the integrated volume method. *Journal Of Aerosol Science*, 39:876–887, 2008.

Sergei S Sazhin. Modelling of fuel droplet heating and evaporation: Recent results and unsolved problems. *Fuel*, 196:69–101, 2017.

J. H. Seinfeld and S. N. Pandis. *Atmospheric Chemistry and Physics: From Air Pollution to Climate Change*. John Wiley & Sons, 2006.

Manish Shrivastava, Christopher D Cappa, Jiwen Fan, Allen H Goldstein, Alex B Guenther, Jose L Jimenez, Chongai Kuang, Alexander Laskin, Scot T Martin, Nga Lee Ng, et al. Recent advances in understanding secondary organic aerosol: Implications for global climate forcing. *Reviews of Geophysics*, 55(2):509–559, 2017.

James S Tanton. *Encyclopedia of mathematics*. Infobase Publishing, 2005.

Olli-Pekka Tikkanen, Väinö Hämäläinen, Grazia Rovelli, Antti Lipponen, Manabu Shiraiwa, Jonathan P Reid, Kari EJ Lehtinen, and Taina Yli-Juuti. Optimization of process models for determining volatility distribution and viscosity of organic aerosols from isothermal particle evaporation data. *Atmospheric Chemistry and Physics*, 19(14):9333–9350, 2019.

Pauli Virtanen, Ralf Gommers, Travis E. Oliphant, Matt Haberland, Tyler Reddy, David Cournapeau, Evgeni Burovski, Pearu Peterson, Warren Weckesser, Jonathan Bright, Stéfan J. van der Walt, Matthew Brett, Joshua Wilson, K. Jarrod Millman, Nikolay Mayorov, Andrew R. J. Nelson, Eric Jones, Robert Kern, Eric Larson, C J Carey, İlhan Polat, Yu Feng, Eric W. Moore, Jake VanderPlas, Denis Laxalde, Josef Perktold, Robert Cimrman, Ian Henriksen, E. A. Quintero, Charles R. Harris, Anne M. Archibald, Antônio H. Ribeiro, Fabian Pedregosa, Paul van Mulbregt, and SciPy 1.0 Contributors. SciPy 1.0: Fundamental Algorithms for Scientific Computing in Python. *Nature Methods*, 17:261–272, 2020. doi: 10.1038/s41592-019-0686-2.

Wes McKinney. Data Structures for Statistical Computing in Python. In Stéfan van der Walt and Jarrod Millman, editors, *Proceedings of the 9th Python in Science Conference*, pages 56 – 61, 2010. doi: 10.25080/Majora-92bf1922-00a.

S1 Supplemental Material

S1.1 Derivation of main equations

Let us consider a general case of a particle consisting of a non-volatile and inert core that is covered with a mixture of volatile compounds that do not interact with the core in any way. Let us define the initial particle diameter as d_0 and the diameter of the non-volatile core as d_n. Let the density of the particle prior to evaporation be ρ_0, that of the volatile mixture be ρ_v, and that of the core ρ_n. The total particle mass prior to evaporation, $m_{t,0}$ is:

$$m_{t,0} = \frac{\pi}{6}\left(\rho_n d_n^3 + \rho_v\left(d_0^3 - d_n^3\right)\right) \tag{S1}$$

The initial density of the particle, i.e., before its evaporation, is:

$$\rho_0 = \frac{\rho_n d_n^3 + \rho_v\left(d_0^3 - d_n^3\right)}{d_n^3 + (d_0^3 - d_n^3))} \tag{S2}$$

During particle evaporation, its diameter will shrink to d, at which point the mass of the volatile mixture, m_v is:

$$m_v = \frac{\pi}{6}\rho_v\left(d^3 - d_n^3\right) \tag{S3}$$

Now let us consider an equation that describes the mass loss rate of compound i in the volatile mixture during its evaporation in vapor-free conditions (i.e., there is no vapor accumulation during evaporation):

$$\frac{\mathrm{d}m_i}{\mathrm{d}t} = -2\pi D_i d F(d) K(d) C_i \frac{m_i}{m_v}, \tag{S4}$$

in which t is time, D_i is the gas phase diffusion coefficient of the compound, C_i is its saturation vapor concentration. $F(d)$ and $K(d)$ are the Fuchs-Sutugin and Kelvin corrections, respectively. The last term in this equation denotes the effect of Rault's law and is equal to the molar fraction of the compound in the volatile mixture assuming that all compounds in the mixture have the same molecular weight.

$$\begin{aligned}\frac{\mathrm{d}m_i}{\mathrm{d}t} &= -\frac{12 D_i C_i}{\rho_0 d_0^2}\frac{d}{d_0}F(d)K(d)\frac{\rho_0 \pi d_0^3}{6}\frac{m_i}{m_v} \\ &= -\tau_i^{-1}\frac{d}{d_0}F(d)K(d)\frac{m_{t,0}}{m_v}m_i,\end{aligned} \tag{S5}$$

where τ_i is the characteristic time:

$$\tau_i = \frac{\rho_0 d_0^2}{12 D_i C_i}. \tag{S6}$$

Using Eqs.S1 and S3, as well as dividing each side of Eq.S5 by the initial mass of component i ($m_{i,0}$), we obtain:

$$\frac{1}{m_{i,0}}\frac{\mathrm{d}m_i}{\mathrm{d}t} = \frac{\mathrm{d}x_i}{\mathrm{d}t} = -\tau_i^{-1}\frac{d}{d_0}F(d)K(d)\frac{m_{t,0}}{m_v}\frac{m_i}{m_{i,0}} \tag{S7}$$

$$= -\tau_i^{-1}\ \frac{\rho_n d_n^3 + \rho_v\left(d_0^3 - d_n^3\right)}{\rho_v d_0}\ \frac{d\,F(d)K(d)}{d^3 - d_n^3}x_i, \tag{S8}$$

where x_i is the mass fraction remaining of compound i ($x_i = m_i/m_{i,0}$). This can be re-written as:

$$\frac{\mathrm{d}x_i}{\mathrm{d}t} = -\tau_i^{-1}\ \left(1 + z_n\left(\frac{\rho_n}{\rho_v} - 1\right)\right)\frac{z^{1/3}}{z - z_n}\ F(z, d_0)K(z, d_0)x_i, \tag{S9}$$

where $z = (d/d_0)^3$ is the volume fraction remaining and $z_n = (d_n/d_0)^3$ is the initial volume fraction of the non-volatile material. Since F and K depend on d, d_0 needs to be specified in addition to z.

This can be expressed in the form of $\log(x_i)$:

$$\frac{\mathrm{d}\log(x_i)}{\mathrm{d}t} = -\tau_i^{-1}\ \left(1 + z_n\left(\frac{\rho_n}{\rho_v} - 1\right)\right)\frac{z^{1/3}}{z - z_n}\ F(z, d_0)K(z, d_0), \tag{S10}$$

If there is no non-volatile core, Eq.S10 reduces to:

$$\frac{\mathrm{d}\log(x_i)}{\mathrm{d}t} = -\tau_i^{-1}\ \frac{F(z, d_0)K(z, d_0)}{z^{2/3}}. \tag{S11}$$

The relationship between the volume fraction remaining, z, and the MFR of individual components can be found in the following way. First, we should note that the mass of the volatile material at any time is:

$$m_v = \sum_i m_i = \sum_i x_i m_{i,0} = m_{v,0}\sum_i x_i f_i \tag{S12}$$

Combining this with EquationS3, we obtain:

$$\frac{\pi\rho_v}{6}\left(d^3 - d_n^3\right) = m_{v,0}\sum_i x_i f_i \tag{S13}$$

$$d^3 - d_n^3 = \frac{6}{\pi\rho_v}m_{v,0}\sum_i x_i f_i \tag{S14}$$

$$d^3 = \frac{6}{\pi\rho_v}\frac{\pi\rho_v}{6}\left(d_0^3 - d_n^3\right)\sum_i x_i f_i + d_n^3 \tag{S15}$$

$$d^3 = \left(d_0^3 - d_n^3\right)\sum_i x_i f_i + d_n^3 \tag{S16}$$

$$z = (1 - z_n)\sum_i x_i f_i + z_n \tag{S17}$$

S1.2 Numerical modeling

Eq.S7 can be used to numerically model both the time evolution of the MFR of individual compounds in the mixture and the particle size or its mass.

For a particle without a non-volatile core, the overall MFR, i.e., the ratio of the particle mass to its original value is equal to $\sum(f_i x_i)$, where f_i is the original VBS (mass fractions of individual compounds in the particle before evaporation). The particle diameter at any time is equal to $d = d_0(\sum(f_i x_i))^{1/3}$. Thus, to model the time evolution of x_i, one needs the corresponding set of the characteristic times, the initial diameter, as well as the parameters needed to calculate the Fuchs-Sutugin and Kelvin correction factors. Once the x_i are calculate, the corresponding particle size and mass can be calculated via the overall MFR.

S1.3 Effect of the temperature dependence of the Kelvin term

As discussed in Section 2.3, the Kelvin term retains an explicit temperature dependence, which is accounted for by evaluating it at the local temperature of each measurement. Figure S1 illustrates the consequence of neglecting this dependence by evaluating the Kelvin term at a single reference temperature instead. The two treatments were applied to the same synthetic thermodenuder measurements as in Section 4.3, retaining in both cases the temperature dependence of the saturation concentration. When the Kelvin term is evaluated at a single reference temperature, the retrieval error grows several times faster with surface tension, and at high surface tension the retrieved VBS is visibly biased relative to the prescribed one. Evaluating the Kelvin term at the local temperature of each measurement removes this bias.

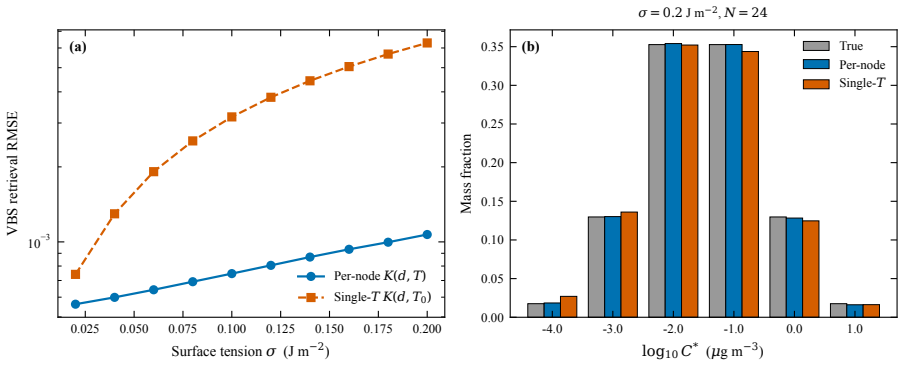

Figure S1: Effect of the temperature dependence of the Kelvin term on the retrieved VBS. (a) RMSE of the retrieved VBS as a function of surface tension when the Kelvin term is evaluated at the local temperature of each measurement (per-node) and at a single reference temperature (single-T), at a fixed number of temperature steps. (b) VBS retrieved with the two treatments at a high surface tension, compared to the true VBS.